12-1-2013

Targeted loss of the ATR-X syndrome protein in the limb mesenchyme of mice causes brachydactyly

Lauren A. Solomon
Western University

Bailey A. Russell
Western University

L. Ashley Watson
Western University

Frank Beier
Children's Health Research Institute, London, ON

Nathalie G. Bérubé
Western University, nberube@uwo.ca

Human Molecular Genetics, 2013, Vol. 22, No. 24 **5015–5025**
doi:10.1093/hmg/ddt351
Advance Access published on July 25, 2013

Targeted loss of the ATR-X syndrome protein in the limb mesenchyme of mice causes brachydactyly

Lauren A. Solomon[1,2,3], Bailey A. Russell[4], L. Ashley Watson[1,2,3], Frank Beier[3,4,*] and Nathalie G. Bérubé[1,2,3,*]

[1]Department of Paediatrics and [2]Department of Biochemistry, The University of Western Ontario, London, Ontario, Canada N6C 2V5, [3]Children's Health Research Institute, London, Ontario, Canada N6C 2V5 and [4]Department of Physiology and Pharmacology, The University of Western Ontario, London, Ontario, Canada N6A 5C1

Received June 17, 2013; Revised and Accepted July 22, 2013

ATR-X syndrome is a rare genetic disorder caused by mutations in the *ATRX* gene. Affected individuals are cognitively impaired and display a variety of developmental abnormalities, including skeletal deformities. To investigate the function of ATRX during skeletal development, we selectively deleted the gene in the developing forelimb mesenchyme of mice. The absence of ATRX in the limb mesenchyme resulted in shorter digits, or brachydactyly, a defect also observed in a subset of ATR-X patients. This phenotype persisted until adulthood, causing reduced grip strength and altered gait in mutant mice. Examination of the embryonic ATRX-null forelimbs revealed a significant increase in apoptotic cell death, which could explain the reduced digit length. In addition, staining for the DNA damage markers γ-histone 2A family member X (γ-H2AX) and 53BP1 demonstrated a significant increase in the number of cells with DNA damage in the embryonic ATRX-null forepaw. Strikingly, only one large bright DNA damage event was observed per nucleus in proliferating cells. These large γ-H2AX foci were located in close proximity to the nuclear lamina and remained largely unresolved after cell differentiation. In addition, ATRX-depleted forelimb mesenchymal cells did not exhibit hypersensitivity to DNA fork-stalling compounds, suggesting that the nature as well as the response to DNA damage incurred by loss of ATRX in the developing limb fundamentally differs from other tissues. Our data suggest that DNA damage-induced apoptosis is a novel cellular mechanism underlying brachydactyly that might be relevant to additional skeletal syndromes.

INTRODUCTION

Alpha-thalassemia mental retardation syndrome, X-linked (ATR-X [MIM 301040]) is a rare genetic disorder caused by mutations to the *ATRX* gene (1). Manifestations of the disease include intellectual disabilities, severe developmental delay, facial dimorphisms, urogenital abnormalities and skeletal deformities (2,3). The latter include brachydactyly, clinodactyly, tapering of the fingers, overlapping digits, and foot deformities. Approximately two-thirds of patients have short stature (2,3). This X-linked syndrome predominantly affects males, whereas carrier females are mostly asymptomatic, presumably due to skewed X-inactivation (3,4). Many ATR-X patients have α-thalassemia caused by impaired production of the α-globin gene leading to unstable tetramers of β-globin chains, or HbH inclusions, in the blood (1,5).

The ATRX protein contains two highly conserved domains where the majority of disease-causing mutations are located. A plant homeodomain-type zinc finger motif, also called the ADD domain, mediates binding to histone H3 trimethylated at lysine 9 and unmethylated at lysine 4 (6–8). ATRX also contains a Sucrose non-fermenting 2 (SNF2)-type DNA-dependent adenosine triphosphate (ATP)ase domain in the C-terminal portion of the protein (3,9). SNF2 proteins are a family of helicase-like proteins that can hydrolyse ATP to remodel chromatin or help repair DNA damage (10).

The ATRX protein interacts with the heterochromatin protein 1 alpha and the Fas death domain-associated protein (DAXX), proteins located at heterochromatin and promyelocytic leukemia nuclear bodies (11). The DAXX/ATRX complex deposits the histone variant H3.3 at telomeres and at pericentromeric

*To whom correspondence should be addressed. Tel: +1 5196858500 (N.G.B.)/+1 5196612111 (F.B.); Fax: +1 5196858616 (N.G.B.)/+1 5198502459 (F.B.); Email: nberube@uwo.ca (N.G.B.)/fbeier@uwo.ca (F.B.)

heterochromatin and can modulate transcription from these highly repetitive genomic regions (12,13).

Emerging evidence indicates that ATRX is required to maintain genomic integrity. Depletion of ATRX in human somatic cells by RNA interference caused mitotic defects including chromosome cohesion, congression and segregation defects (14). In the mouse, conditional inactivation of *Atrx* in forebrain, muscle and Sertoli cells was reported to induce cell death (15–18). Surprisingly, we showed that deletion of *Atrx* in chondrocytes did not result in increased cell death, demonstrating that the outcome of ATRX deficiency differs across cell types (19). In mouse embryonic stem cells, ATRX depletion results in reduced histone H3.3 deposition at telomeres and in telomere-dysfunction phenotypes (6). Our group and others have shown that increased instability at telomeres associated with ATM activation occurs upon ATRX inactivation (18,20). We demonstrated that combined deletion of the *p53* and *Atrx* genes in the developing nervous system abolishes embryonic cell death, leading to an accumulation of neurons with DNA damage. Thus, loss of ATRX causes DNA damage, which triggers p53-dependent apoptotic cell death (20,21). ATRX-deficient cells are hypersensitive to fork-stalling agents, but not to gamma irradiation, suggesting that loss of ATRX specifically promotes DNA replication stress (20,22). This is supported by the co-localization of DNA damage foci with the replication marker PCNA in ATRX-null cells (18,20). Leung *et al*. demonstrated that ATRX is recruited to sites of DNA damage with the MRN complex and promotes restart of stalled forks (22). Finally, we were able to show that neuroprogenitors lacking ATRX accumulate more DNA damage and display reduced survival upon treatment with telomestatin, a G-quadruplex ligand, suggesting that replication stress induced by ATRX deficiency is linked to G-quadruplex stability (20).

Given the high frequency of skeletal abnormalities reported in ATR-X syndrome patients, especially in hands and feet, we hypothesized that ATRX may protect cells in the developing limbs from endogenous DNA replication damage or that it might control pathways required for proper development of the skeleton in the distal limbs. We find that conditional deletion of *Atrx* in limb bud mesenchyme causes a specific and significant shortening of the distal phalanges. Embryonic ATRX-null limb bud cells display one large γ-histone 2A family member X (γ-H2AX)/53BP1-positive focus adjacent to the nuclear membrane in each nucleus that persists upon cell differentiation. While the majority of cells seem to be able to differentiate despite unrepaired DNA damage, we detected an increase in apoptotic cell death that might explain the reduced digit length in the *Atrx*(Prx1) cKO mice. Our findings suggest that apoptosis in response to DNA damage is a novel mechanism giving rise to brachydactyly.

RESULTS

Generation of mice lacking *Atrx* specifically in the limb mesenchyme

We utilized the Cre-LoxP system to generate mice lacking the *Atrx* gene in early limb bud mesenchyme. Homozygous floxed $Atrx^{loxP}$ female mice (16) were mated with male Tg(Prx1-cre)1Cjt mice expressing Cre recombinase under the control of the *Prx1* promoter that drives recombination in early limb bud mesenchyme (23). Since *Atrx* is located on the X chromosome, males resulting from this cross carry one copy of the *Atrx* gene that contains the loxP sites. Cre-positive males are conditionally ATRX-null and are referred to as *Atrx*(Prx1) cKO. All animals in this study were from the first generation of this cross.

Reverse transcriptase PCR (RT–PCR) analysis of *Atrx* expression in embryonic day 16.5 forepaws shows a reduction in wild-type *Atrx* mRNA and the presence of low levels of a shorter transcript resulting from the recombination of exon 18 in mutant limb mesenchyme. The amount of this truncated RNA was greatly reduced, confirming that the RNA is unstable and is equivalent to a null mutation (Fig. 1A), as we have shown previously (16). ATRX protein was detected at high levels in the

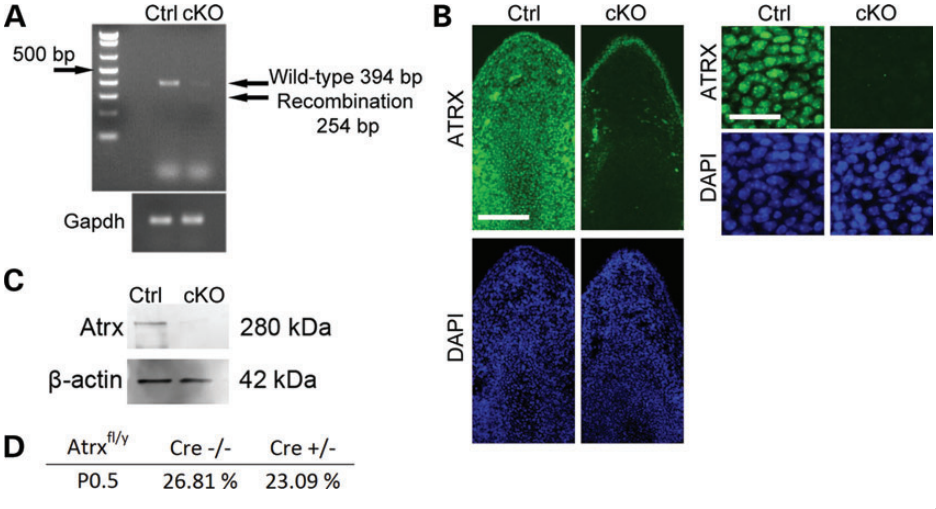

Figure 1. *Atrx* is deleted in the forelimbs of *Atrx*(Prx1) cKO mice. (**A**) RT–PCR analysis of RNA isolated from embryonic forelimbs of $Atrx^{fl/yPrxcre+}$ males *Atrx*(Prx1) cKO (KO) and control littermates (Ctrl). Amplification was performed with primers flanking the loxP sites, in introns 17 and 20. Recombined RNA in *Atrx*(Prx1) cKO is unstable and degraded. (**B**) Cryosections of E15.5 forelimb tissue were stained for ATRX protein. *Atrx*(Prx1) cKO mice lack ATRX in the nucleus of all mesenchyme tissues. Scale bar: 200 μm (representational high-resolution image: 50 μm) (**C**) Immunoblot of proteins isolated from E15.5 forelimbs shows loss of ATRX protein in *Atrx*(Prx1) cKO mice. (**D**) *Atrx*(Prx1) cKO mice are born at normal Mendelian ratios, with no associated lethality.

control, but was absent in the cartilage and pre-cartilaginous condensations of the *Atrx*(Prx1) cKO mice (Fig. 1B and C). ATRX protein is retained in the nucleus of epithelial cells of the limb, confirming that *Cre* activity is indeed limited to the limb mesenchyme when expressed under the control of the *Prx1* promoter. Mutant *Atrx*(Prx1) cKO mice were born at normal Mendelian ratios (Fig. 1D) and had a normal birth weight (Supplementary Material, Fig. S1). They lived beyond the age of one year and were fertile.

Mice lacking *Atrx* in the forelimb mesenchyme develop brachydactyly

To evaluate the phenotypes of *Atrx*(Prx1) cKO mice, forelimbs were collected and patterns of cartilage and mineralized bone were examined at various embryonic times by alcian blue/alizarin red staining (respectively). Embryonic forepaws showed no difference between control and mutant mice at embryonic day 14.5 (Fig. 2A). However, at E15.5, we observed that the condensation of the anlage for phalange 2 was reduced in size (Fig. 2B). A more severe delay was seen at E16.5. The paws in controls had four cartilage condensations and establishment of phalange 3, while these condensations were significantly shortened or absent in the Atrx mutant littermates (Fig. 2C). At this stage of embryonic development, the *Atrx*(Prx1) cKO embryos displayed a significant shortening of total digit length, with smaller ossified elements in the distal phalanges. This phenotype is consistent with brachydactyly in ATR-X syndrome (24).

Whole skeletal preparations were obtained from newborn, weanling (P21) and adult mice. Distal phalanges in *Atrx*(Prx1) cKO mice displayed reduced or absent mineralization at birth and were significantly shorter than the phalanges of control littermates (Fig. 3A). This phenotype was evaluated at P21, and we found that the shortening of the distal phalanges persisted even after complete mineralization of the paw (Fig. 3B). Proximal phalanges (metacarpals and phalange 1) were not affected, whereas the distal phalanges (phalanges 2 and 3) are significantly shorter in all digits. Microcomputed tomography analysis of P21 forepaws was performed and showed that the shape of the fingers and claws is altered. Fingers displayed abnormal flexation, whereas mineralization and cortical thickness are not affected (Fig. 3C). Adult *Atrx*(Prx1) cKO mice still exhibit brachydactyly at 1 year of age (Fig. 3D), indicating that the early phenotypes do not simply represent a delay in development

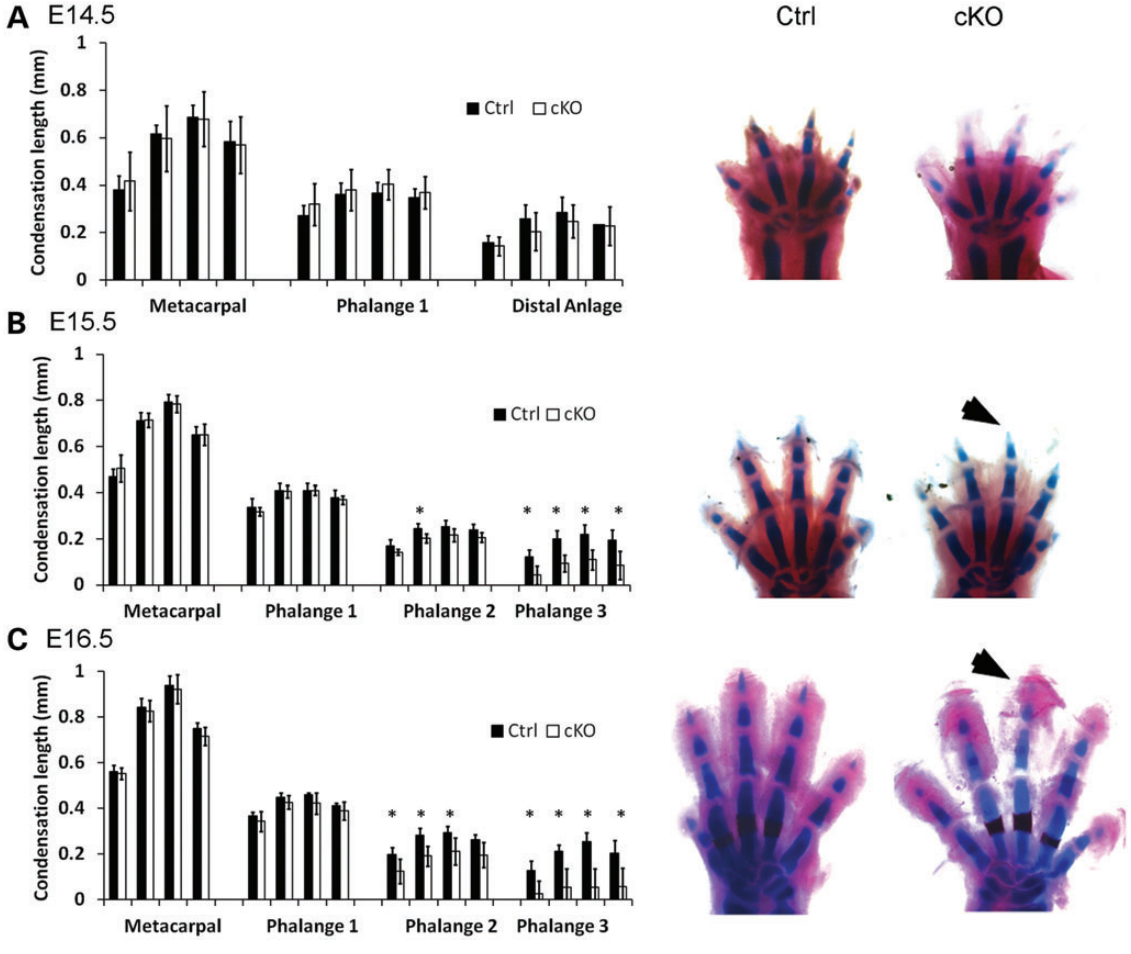

Figure 2. *Atrx*(Prx1) cKO digit defects appear at embryonic day 15.5. (**A**) Phalange length measurements from embryonic day 14.5 $Atrx^{fl/yPrxcre-}$ (CTRL) and *Atrx*(Prx1) cKO (KO) mice. No differences are seen in the length of cartilaginous condensations in the forelimb. (**B**) Phalange length measurements at embryonic day 15.5. cKO mice exhibit shortening of terminal phalanges. (**C**) Phalange length measurements from embryonic day 16.6. All distal phalanges are significantly shortened in mutant mice. $^{*}P < 0.05$, $n = 3$.

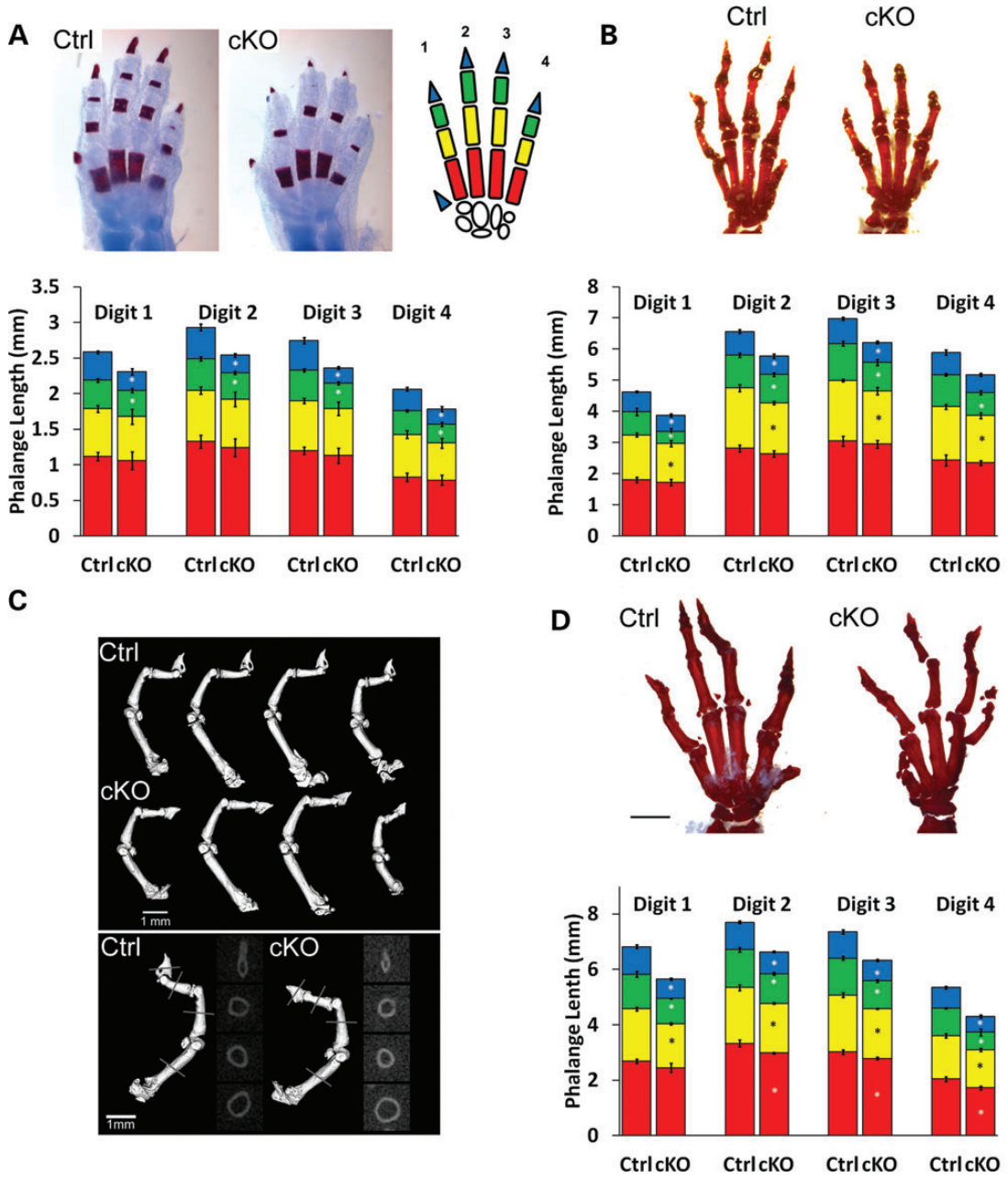

Figure 3. *Atrx*(Prx1) cKO mice show brachydactyly. (**A**) Skeletal stains of control (Ctrl) and *Atrx*(Prx1) cKO (KO) newborn (P0.5) forelimbs. Cartilage is stained in blue, mineralized tissue is stained in red. Proximal bones (metacarpals and the first phalange) were not affected in the mutant; however, distal phalanges were significantly shortened and lacked mineralization. $^*P < 0.05, n = 3$ (**B**) Skeletal stains of control (Ctrl) and *Atrx*(Prx1) cKO (KO) weanling (P21) forelimbs. Significant shortening is observed in all phalanges, excluding the metacarpals $^*P < 0.05, n = 3$. (**C**) MicroCT isosurfaces of P21 digits. *Atrx*(Prx1) cKO digits lack flexation of the terminal phalanges, and have short, malformed claws. Cortical thickness was unaffected. Scale bar: 1 mm (**D**) Skeletal stains of control (Ctrl) and *Atrx*(Prx1) cKO (KO) adult (1 year old) forelimbs. Mineralized tissue is stained in red. Significant shortening is observed in all phalanges. $N = 3$ for all time points, $^*P < 0.05$.

but rather a permanent phenotype. The proximal bones of mutant forelimbs (humerus, radius, ulna) did not show any abnormalities at any investigated age.

Cell death is increased in the *Atrx*(Prx1) cKO embryonic limb bud mesenchyme

The observation that *Atrx*(Prx1) cKO mice have shorter digits suggests a reduction in cell numbers during embryogenesis, which could be explained by reduced proliferation or increased cell death. Proliferation was assessed using Ki67 staining (a marker of proliferation). Quantification of Ki67-positive cells in the distal portions of control and *Atrx*(Prx1) cKO digits showed that cell proliferation is not different between genotypes at E13.5 and E15.5, which represent times before and after the appearance of the phenotype, respectively (Fig. 4).

We next assessed the level of apoptosis by the TUNEL assay and staining for activated caspase 3 at E13.5. As expected, we

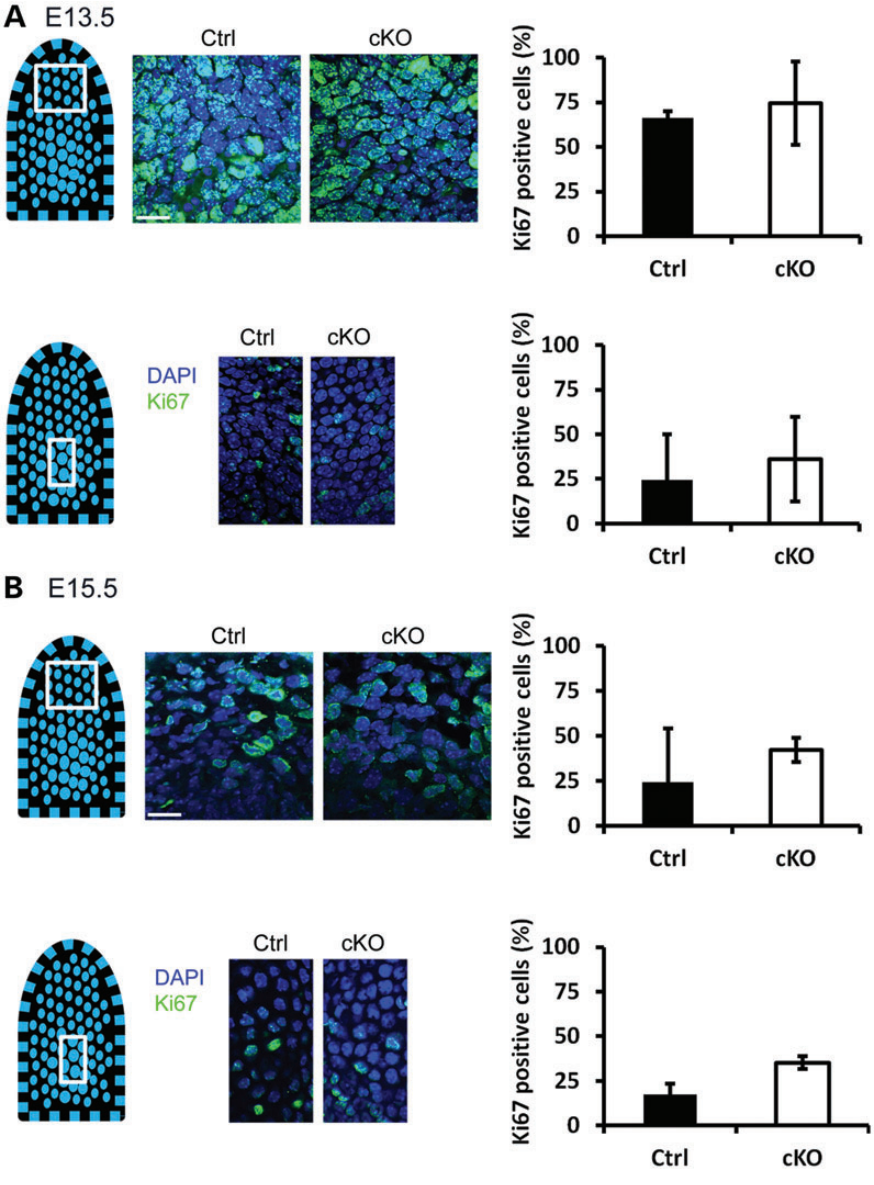

Figure 4. Proliferation is unchanged in the *Atrx*(Prx1) cKO embryonic limb bud. Immunofluorescent stains for the S-phase marker Ki67 in embryonic day 13.5 (**A**) and 15.5 (**B**) forelimb cryosections. More Ki67+ cells are present in the highly proliferative distal tip when compared with the differentiated digit ray, but no significant change is observed between genotypes. Scale bar: 20 μm, Error bars = SD, $n = 3$.

observed clusters of apoptotic cells in the interdigital mesenchyme in both genotypes. We also observed an increase in the number of apoptotic cells in the mutant compared with control digits. At E13.5, there was a 6.9-fold increase in apoptotic cells in the *Atrx*(Prx1) cKO ($P = 0.038$, $n = 4$), and a 4.8-fold increase in the number of cells containing activated caspase 3 ($P = 0.004$, $n = 4$) (Fig. 5). At E15.5 there was a significant 3.8-fold increase in apoptotic cells in the *Atrx*(Prx1) cKO ($P = 0.028$, $n = 3$) (Supplementary Material, Fig. S2).

Increased level of γ-H2AX foci in Atrx-null embryonic limb bud mesenchyme and chondrocytes

As we and others previously reported increased levels of DNA damage upon loss of *Atrx* (18,20), we examined *Atrx*(Prx1) cKO forelimbs for evidence of DNA damage. We stained embryonic limb cryosections from E12.5 to E17.5 with an antibody against phosphorylated γ-H2AX, a marker of DNA double-strand breaks (DSBs). Confocal imaging and quantification at E13.5 and E15.5 showed a significant increase in the number of cells harboring γ-H2AX foci in the forelimb mesenchyme of *Atrx*(Prx1) cKO mice (Fig. 6A and B) and cartilaginous digit rays (Supplementary Material, Fig. S3). To confirm this result, we co-stained cryosections with 53BP1, a DNA damage response protein that promptly re-localizes to damaged sites. We observed a higher number of 53BP1 foci in mutant forepaws that largely overlapped with the γ-H2AX foci (Fig. 6C). In the limb buds of heterozygous female embryos, *Atrx* is deleted in ~50% of cells, as expected from a random pattern of X-inactivation. Forelimb tissue of heterozygote female mice at

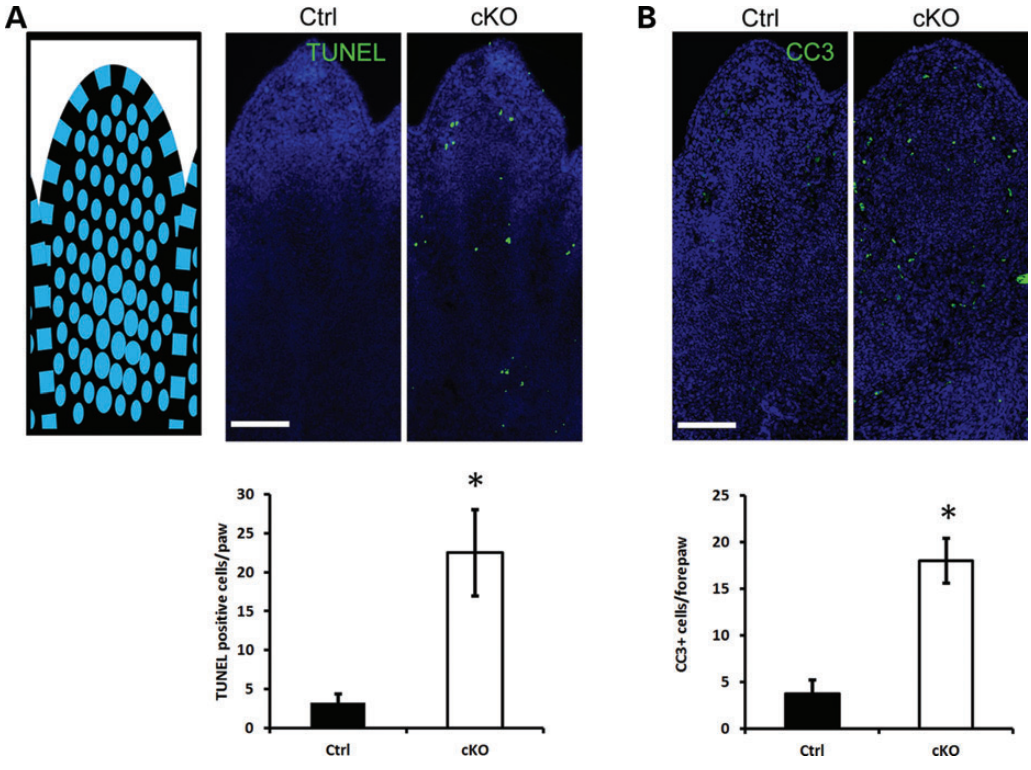

Figure 5. Cell death is increased in the *Atrx*(Prx1) cKO embryonic limb bud. Fluorescent TUNEL and activated caspase 3 stains of frozen sections for embryonic day 13.5 forelimbs. (**A**) At E13.5, more TUNEL positive nuclei are observed per digit tip in mutant forelimb sections ($n = 4$). (**B**) *Atrx*(Prx1) cKO embryonic limb buds contain significantly more cells containing activated caspase 3. Scale bar: 200 μm error bars = SEM.

E13.5 had γ-H2AX foci in 17% of cells (Supplementary Material, Fig. S4), but <2% of ATRX+ cells contained DNA damage foci. These findings suggest that DNA damage incurred is due to a cell-autonomous effect of Atrx loss.

Surprisingly, the γ-H2AX staining in *Atrx*(Prx1) cKO cells appeared as one discrete, bright focus in the nucleus (Fig. 6D). Moreover, staining of the sections with an antibody that recognizes lamin B demonstrates that the large majority of the DNA damage foci are located in close proximity to the nuclear lamina, which was confirmed by measurements of distance of the foci to the nuclear lamina using confocal microscopy (Fig. 6D and E). Interestingly, no increase in γ-H2AX staining was observed in male embryos when the *Atrx* gene was inactivated using the cartilage-specific Col2-Cre driver line (Supplementary Material, Fig. S5).

Atrx-deficient forelimb mesenchyme cells are not hypersensitive to hydroxyurea treatment

Control and *Atrx*(Prx1) cKO embryonic forelimbs were cultured and treated with increasing concentrations of the fork-stalling compound hydroxyurea (HU) for 24 h to determine whether ATRX-deficient limb bud cells are more sensitive to replication stress, as has been reported for other cell types (20–22). Twenty-four or 48 h after end of treatment, cell viability was assessed by MTT assays. γ-H2AX staining increased in a dose-dependent manner in response to HU treatment. However, we observed that cells of all genotypes showed a similar reduction in viability in response to HU (Supplementary Material, Fig. S6).

Reduced forelimb function and shorter stride length in Atrx cKO mice

To determine whether the brachydactyly phenotype observed in the *Atrx*(Prx1) cKO (Fig. 7A) had any functional consequence, we evaluated various parameters of forelimb function and gait. We found that the maximal grip strength values of adult *Atrx*(Prx1) cKO mice were significantly lower than those of control littermates (Fig. 7B), reflecting a loss of forelimb function that coincides with shortening of the phalanges. Next, we utilized the Catwalk system to analyze gait parameters in freely ambulating mice. The spatial relationship between paw prints was used to determine stride length and walking pattern. Forelimb stride length was reduced in *Atrx*(Prx1) cKO mice compared with control littermates (45.65 ± 3.06 mm versus 50.09 ± 2.64 mm, $P < 0.05$). Hind limb stride length was also reduced (45.45 ± 2.94 mm versus 50.23 ± 2.93 mm, $P < 0.05$), despite the absence of any morphological changes in the hind limbs of mutant mice (Fig. 7C). Conversely, the regularity index of footfall patterns did not vary between genotypes, indicating that mutants had a normal walking pattern and showed no instability or impairment in gait (Supplementary Material, Fig. S7A and B). Additionally, there was no significant variation in base of support or swing duration when walking (Supplementary Material, Fig. S7C and D).

DISCUSSION

Our study shows that loss of ATRX in early limb mesenchyme leads to brachydactyly and smaller digits, associated with

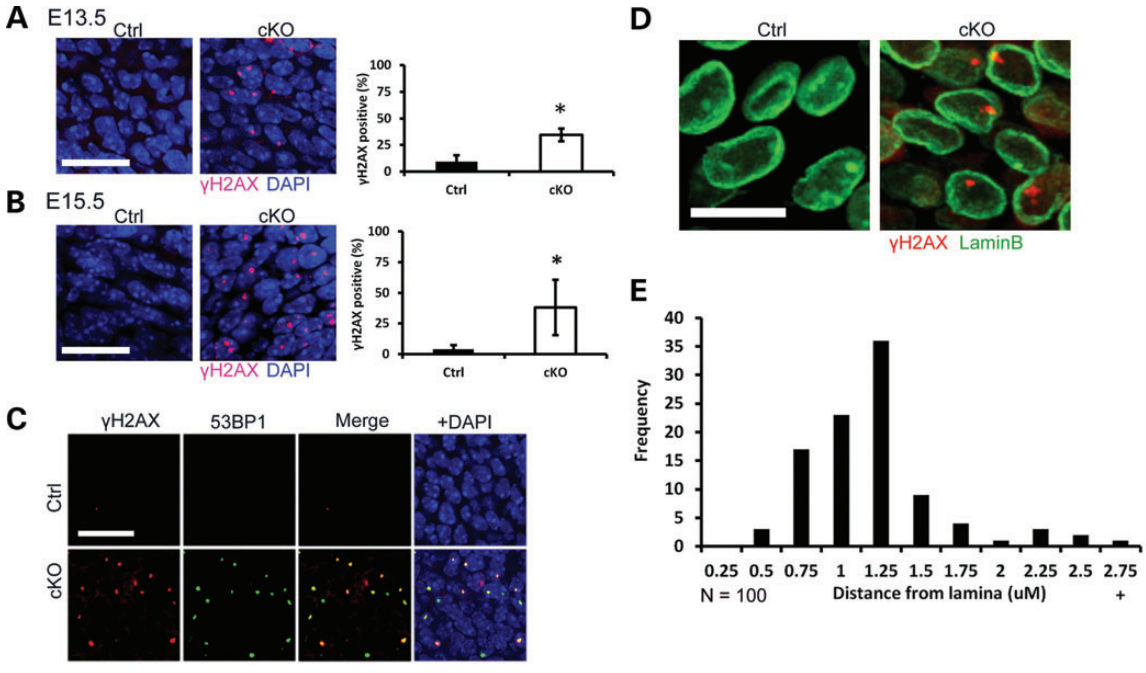

Figure 6. ATRX-deficient limb buds have increased levels of DNA double-strand breaks. (**A**) Immunofluorescent stains for the phosphorylated histone gamma-H2A.X (γ-H2AX) in embryonic day 13.5 forelimb sections. γ-H2AX signal frequently appears in the mutant nuclei as a single bright focus which is absent in the control. Expression of γ-H2AX was similar between distal phalange tips and differentiated digit rays. Scale bar: 50 μm (**B**) Immunofluorescent stains for γ-H2AX in embryonic day 15.5 forelimb section demonstrating persistence of the γ-H2AX foci within the nucleus of *Atrx*(Prx1) cKO cells. Scale bar: 50 μm (**C**) Immunofluorescent stains for γ-H2AX and 53BP1 in embryonic day 13.5 forelimb sections. Sites of γ-H2AX signal co-localize with 53BP1 in all parts of the forelimb. Scale bar: 50 μm (**D**) Immunofluorescent staining for Lamin B and γ-H2AX, demonstrating large DNA damage foci located in close proximity to the nuclear lamina. Scale bar: 10 μm (**E**) Quantification of distance between the center of the bright γ-H2AX focus and the nearest nuclear lamina.

DNA damage and apoptosis. Specifically, brachydactyly occurred as shortening of the distal phalanges of the forelimb, beginning at E15.5. *Atrx* has previously been deleted in the early developing cartilage without phenotypic consequence, raising questions about the cell types responsible for the skeletal abnormalities in ATR-X patients (19). We demonstrate here that loss of ATRX in mesenchymal precursor cells prior to differentiation into cartilage gives rise to one skeletal phenotype observed in ATR-X syndrome patients. Furthermore, our model suggests that apoptosis in response to DNA damage is a new molecular and cellular mechanism responsible for brachydactyly. This is distinct from other forms of brachydactyly, many of which are due to mutations in key developmental signaling genes, such as components of the hedgehog, Wnt or TGF-beta family pathways or Hox genes (25,26).

This model, unlike loss of ATRX in developing cartilage (19), deletes *Atrx* early in limb development and leads to a more severe phenotype. This suggests that ATRX function is more critical in mesenchymal precursor cells than in differentiated chondrocytes. In support of this model, we did not observe any DNA damage in our cartilage-specific ATRX-deficient mice. In our experiments, the distal portions of the digit are first to show significant shortening, and during post-natal development the affected mice do not catch up to littermates.

One question addressed by this study is whether loss-of-function of ATRX has a direct effect in the developing skeleton. The observed brachydactyly is likely to be a direct effect of ATRX in the limb bud, rather than a secondary effect of ATRX loss in another tissue, as this model uses a cre-lox system specific for the early forelimb. The hind limbs were not affected in the mutant mice, which was expected since Prx-cre activity is limited in the hind limb compared with the forelimb (23). Our findings demonstrate that not only does loss of ATRX in the forelimb mesenchyme have direct effects on skeletal development, but it also has wide-reaching effects on the physiology of the adult animal. Adult mutant mice retain shortening on the distal phalanges, and have visibly smaller paws than control littermates. Furthermore, the digits in the paws are not flexed normally, and have reduced function. These mice have weaker grip strength due to the smaller digits, an indication that the shorter fingers are more difficult to bend and have limited strength. The reduced function is also observed in the gait of these animals, in which they maintain a normal pattern of walking but take significantly shorter steps.

Prior to the appearance of the phalange shortening, mutant mice display widespread DNA double-strand breaks in limb bud tissue as identified by increased γ-H2AX staining. Previous studies have shown that ATRX is required for maintaining structural integrity of telomeres and depletion of ATRX leads to telomere instability and fusions (6,20). However, in contrast to other models of ATRX deficiency, the DNA damage seen in limb bud cells in our study exhibit two specific characteristics. First, DNA damage occurs as one discrete dot in the nucleus, close to the nuclear periphery. This single focus is unusual, as γH2AX-postive DNA damage has a more speckled or diffuse appearance in other ATRX-null tissues (6,18,20). It is not clear at this point whether the signal we observe is from one chromosomal site or from an amalgamation of several damaged sites at the nuclear

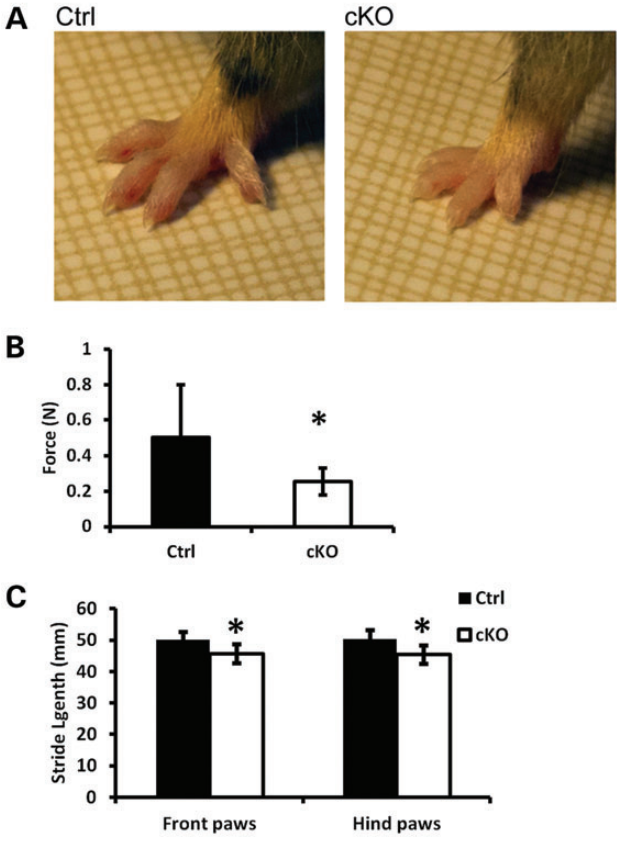

Figure 7. Reduced forelimb function at 1 year of age in *Atrx*(Prx1) cKO mice. (**A**) Characteristic forelimb appearance of Ctrl and *Atrx*(Prx1) cKO mice showing shortened fingers and a smaller paw. (**B**) Forelimb grip strength of control and mutant adult mice. Mutant mice exert significantly less force with their forelimbs before releasing the bar. (**C**) Quantification of mouse gait parameters. Stride length of the fore- and hind-paws is shorter in *Atrx*(Prx1) cKO mice.

lamina. It has been shown in budding yeast that numerous domains containing DSBs can merge into one aggregate in the nucleus. In this manner, persistent DSBs and telomeres can be sequestered to the periphery of the nucleus, a common location for dangerous and damaged DNA elements in the genome (27–30). Large DNA damage foci have also been observed in pig skin cells following gamma irradiation: the damage appears initially at multiple sites but after 70 days can be seen as one or a few large nuclear foci (31). In mouse embryonic fibroblasts, the inner nuclear envelope proteins SUN1 and SUN2 have been shown to be important in DNA damage response and possibly play a role in non-homologous end joining repair (32). Mammalian nuclear lamins themselves are also important in nuclear organization and cell-cycle response to DNA damage (33). Thus, persistent DSBs within the nuclei of ATRX-depleted forelimb cells might re-localize to the nuclear periphery, either for sequestering from the rest of the genome, repair or activation of cell-cycle arrest. A second unusual feature of ATRX-deficient limb bud cells is that they are not hypersensitive to HU treatment while ATRX deficiency in neuroprogenitors and other cells leads to increased sensitivity to replication stress-inducing drugs (20,34). In the developing forelimb, the most affected cells at the distal end of the digit are highly proliferative and contribute to lengthening of the digits. Thus, one could have expected these cells to be very sensitive to replication stress, but our data show that loss of ATRX does not increase the sensitivity of these cells to HU treatment. In addition, the level of cell death observed in mutant digits is markedly lower than that seen in the ATRX-null brain (18,20,22). The specific connection between loss of ATRX and DNA damage in limb bud cells, therefore, remains to be explored.

Our studies add to recent publications implicating epigenetic regulators in brachydactyly and skeletal development. Heterozygote mutations in the *HDAC4* gene, encoding a histone deacetylase, have been identified as a cause of brachydactyly type E, and translocation of a gene encoding a long non-coding RNA results in brachydactyly type E as well (35,36). Maybe most closely related to our studies, loss of the single-stranded DNA-binding protein OBFC2B leads to growth delay and skeletal abnormalities due to accumulation of γ-H2AX and apoptosis in the pre-cartilage condensations (37). While OBFC2A, a homologue, is required in many other cell types (37), it appears that the skeletal lineage has developed specific methods of dealing with increased levels of DNA damage during development. A genetic assault, such as the loss of ATRX, is still hazardous in the developing forelimb, but not to the same degree as in the CNS. Thus, our results suggest that the role of ATRX varies between cell types, or alternatively that different cell types utilize distinct mechanisms to maintain genomic integrity.

In summary, by using tissue-specific deletion of *Atrx*, we have recapitulated part of the skeletal phenotype of ATR-X syndrome and found a direct role for ATRX in preventing DNA damage and maintaining cell survival in the highly proliferative developing digit mesenchyme. Our data suggest that DNA damage-induced apoptosis of limb mesenchymal cells can result in brachydactyly, although we cannot exclude contributions of other mechanisms. This model may be functionally relevant to additional brachydactylies and other skeletal dysplasias.

MATERIALS AND METHODS

Mouse husbandry, genotyping and tissue preparation

Mice were housed with a 12-h light–dark cycle, and fed tap water and regular chow ad libitum. Mice conditionally deficient for Atrx in the early limb bud mesenchyme were generated using the 129SV $Atrx^{loxP}$ mice described previously (15,16). $Atrx^{loxP}$ mice were mated to mice expressing transgenic Cre recombinase under the control of the *Prx1* promoter (Prrx1-cre) (23) to generate $Atrx^{loxP/YPrx1Cre+}$ animals lacking ATRX in the developing forelimb. Tg(Prrx1-cre)1Cjt mice were obtained from Jackson Laboratories. For embryonic time points, noon of the day after mating was considered to be E0.5. Genotyping for *Atrx*, *Cre* and Y chromosome was determined by PCR as previously described (16,21). Only male mice were used in studies, with the exception of Supplementary Material, Figure S4 examining heterozygote female mice. Embryonic tissue collected for histology was fixed in PFA overnight at 4°C overnight, then equilibrated in 30% sucrose and embedded in VWR clear frozen section compound over liquid nitrogen. Forelimbs were sectioned at 5 μm and stored at −80°C. All procedures involving animals were conducted in accordance with the regulations of the Animals for Research Act of the Province of Ontario and

approved by the University of Western Ontario Animal Care and Use Committee.

Quantification of skeletal defects

Embryonic forepaws were isolated and dehydrated in 95% ethanol for 24 h, followed by acetone for 24 h. Paws were then stained with 0.015% alcian blue, 0.05% alizarin red and 5% acetic acid in 70% ethanol as described (38). The stained paws were cleared in glycerol/1% KOH (1:1) and stored in glycerol/ethanol (1:1). Adult skeletons were cleaned and stained as described, then cleared in 2% KOH and stored in glycerol/ethanol (1:1). Embryonic forepaws were cleared and imaged using a Nikon SMZ1500 dissecting microscope with a Photometrics (Tucson, AZ) Coolsnap camera using the ImageMaster 5.0 software. Adult phalanges were microdissected and imaged as described. Digit length was measured in ImageJ and analyzed using Graphpad from at least three independent litters at each age.

Microcomputed tomography

Mice were euthanized at P21, forelimbs were dissected and fixed in paraformaldehyde overnight followed by immobilization in agarose. Whole forepaws were scanned on a GE Locus scanner at 80 kV and 0.08 mA with a 0.013 mm^3 voxel resolution with 900 slices per scan. Scans were analyzed using Microview 3D visualization and analysis software (MicroView, Version 2.1.2, GE Healthcare Biosciences), as described (39). Whole forepaw isosurface images were generated by applying a threshold of 932 HU, surface quality factor of 1.00 and a surface decimation factor of 30.

Western blot analysis

Embryonic forelimbs were dissected in PBS into RIPA buffer and homogenized using a fine-gauge needle. SDS–polyacrylamide gel electrophoresis (PAGE) sample buffer (5 μl) was added to samples, followed by boiling for 5 min. Samples were separated by gradient SDS–PAGE (Biorad) and transferred to nitrocellulose membranes (Amersham). Membranes were blocked in 2% BSA and incubated with primary antibodies in accordance with the instructions from the primary antibody supplier. The following antibodies were used; Anti-ATRX (Santa Cruz, #sc-15408,1:1000), mouse anti-β-actin (Sigma-Aldrich, #A2228, 1:10,000), Goat anti-rabbit HRP (Santa Cruz, #sc-2030, 1:5000), Goat anti-mouse HRP (Santa Cruz, #sc-2031, 1:5000). Representative blots from three independent experiments are shown.

Immunofluorescence assays

Proliferating cells were visualized using antibodies for Ki67. Frozen sections were rehydrated and antigens retrieved using 0.1 M sodium citrate. Sections were permeabilized for 1 h with blocking buffer containing 5% goat serum and 0.1% tween-20 in phosphate-buffered saline, followed by overnight incubation with primary antibodies mouse anti-gamma-H2AX (Millipore, #05-636) and either rabbit anti-53BP1 (Cell Signaling, #4937), rabbit anti-ATRX (Santa Cruz, #sc-15408), or rabbit antiKi67 (Abcam, #ab15580) at a concentration of 1:300 in blocking buffer. Antibodies were detected using fluorescently conjugated secondary antibodies, FITC goat anti-rabbit (Biosource, #ALI0408) and Alexa-594 goat anti-mouse (Invitrogen, #A11032) at dilutions of 1:200. Slides were mounted in media containing DAPI (Vectashield) and confocal images were acquired on an Olympus FluoView TV1000 coupled to the IX81 Motorized Inverted System Microscope (IX2 Series). Damage was quantified by a blinded observer within a fixed area of 10 000 μm^2 for digit tips and 5000 μm^2 for digit rays. Counts were averaged from three independent litters at each time point. To assess apoptosis, 5 μm sections from E13.5 and E15.5 mice were used for the TUNEL assay using the Roche *In Situ* Cell Death Detection Kit, Fluorescein according to manufacturer's instructions. Briefly, frozen sections were hydrated in PBS and treated with cold citrate for 2 min. Slides were washed and incubated in the enzyme/label solution mix for 1 h at 37°C, then mounted with DAPI-containing mounting media (Vectashield). Sections were imaged on a Leica DMRA2 automated inverted microscope. Signal was quantified from sections using a fixed area over each digit by a blinded observer. Counts were averaged from at least three independent litters.

Activated caspase 3 was visualized in sections using rabbit anti-cleaved caspase-3 (Cell Signaling, #9664, 1:400 dilution). Cryosections were rehydrated in 1XPBS for 5 min and subjected to antigen retrieval by heating 0.1 M sodium citrate ph6 to 95°. Sections were permeabilized with 1X PBS/0.3% Triton X for 5 min and incubated with primary antibody diluted in 1XPBS/0.3% Triton-X overnight at 4°. Sections were washed 3× with 1× PBS/0.3% Triton X for 5 min each and incubated with goat anti-rabbit Alexa 488 (Molecular Probes, #A-11070, 1:800 dilution) diluted in 1XPBS/0.3% Triton-X for 1 h at RT. Sections were washed 2× with 1× PBS/0.3% Triton × for 5 min each, incubated with 1 μg/μl DAPI/1XPBS for 5 min and washed 3× with 1× PBS/0.3% Triton × for 5 min each. Slides were then mounted using SlowFade Gold (Invitrogen) and imaged using an inverted fluorescence microscope (Leica, DMI6000b).

Immunofluorescence assays were conducted for γ-H2AX and the nuclear envelope marker Lamin-B as described previously (40,41). Nuclear lamina was detected using a goat anti-Lamin-B antibody (Abcam, #ab16048) at a concentration of 1:300, whereas DNA double-strand breaks were visualized with mouse anti-γ-H2AX (Millipore, #05-636) at a concentration of 1:200 in blocking buffer and detected with Alexa-594 donkey anti-mouse (Invitrogen, #A-11005) and FITC donkey anti-goat (Invitrogen, #A-11055) at a concentration of 1:200. Three-dimensional images of nuclei were collected on an Olympus FluoView TV1000 coupled to the IX81 Motorized Inverted System Microscope (IX2 Series) in image stacks captures at 0.25 um Z-sections and deconvoluted in Volocity (PerkinElmer). Measurements were taken from the center of the γ-H2AX focus to the closest nuclear periphery for 100 individual nuclei.

HU treatment and assessment of DNA damage and survival

Primary forelimb mesenchyme was prepared using distal forelimb tissue dissected from E13.5 embryos. Cells were dissociated with collagenase at 37°C for 1 h and plated in DMEM/F12 media supplemented with 10% FBS, 0.25% pen/strep and

0.25% L-glutamate (Gibco). Forelimb mesenchyme cultures were treated with increasing doses of HU (0.05–1 mM) for 24 h, recovered for 24 or 48 h, and cell viability measured by the MTT assay as described (42). Briefly, media containing HU was removed and replaced with fresh media for 24 or 48 h, followed by replacement with media containing 0.5 mg/ml MTT for 4 h. Product was stabilized in DMSO and quantified on a spectrophotometer at 595 nm.

Gait and grip strength analyses

Behavioral assays were performed at the behavioral core facility at the Robarts Research institute (London, ON). Control and mutant mice at P21 and 1 year of age freely ambulated on an illuminated glass platform, and movements were recorded with a high speed camera using the Noldus CatWalk system. After an initial training period, at least three un-interrupted runs were collected from each animal. Each run was analyzed using the Catwalk 7.1 software for classifying foot contacts. Run data for each animal were averaged, and then averages calculated within each genotype. Means were analyzed for statistical differences between genotypes using Student's *t*-test. Mouse forelimb grip strength was assessed using a digital force gauge as described previously (43). Briefly, the animal was grasped by the scruff of the neck in one hand, and the base of the tail in the other. Measurements were recorded on the meter as the subject was allowed to grip, and then was pulled away from, the grip bar. Total peak force was determined from an average of five measurements taken from each animal, and the means of each genotype were compared. Statistical analysis of the means was conducted using Student's *t*-test.

SUPPLEMENTARY MATERIAL

Supplementary Material is available at *HMG* online.

ACKNOWLEDGEMENTS

We thank Drs Douglas Higgs and Richard Gibbons (Weatherall Institute of Molecular Medicine, John Radcliffe Hospital, Oxford, UK) for kindly providing the *Atrx*^{loxP} mice used in this study.

Conflict of Interest statement. None declared.

FUNDING

This work was supported by an operating grant from the Canadian Institutes for Health Research to N.G.B. and F.B. (MOP102539), an Ontario Graduate Studentship (OGS) to L.A.S., Paediatrics Graduate Studentship at the University of Western Ontario, the Curtis Cadman Studentship and Queen Elizabeth II Ontario Graduate Scholarship in Science and Technology (QEIIOGSST) to L.A.W.

REFERENCES

1. Gibbons, R.J., Picketts, D.J., Villard, L. and Higgs, D.R. (1995) Mutations in a putative global transcriptional regulator cause X-linked mental retardation with alpha-thalassemia (ATR-X syndrome). *Cell*, **80**, 837–845.
2. Gibbons, R.J. and Higgs, D.R. (2000) Molecular-clinical spectrum of the ATR-X syndrome. *Am. J. Hum. Genet.*, **97**, 204–212.
3. Gibbons, R.J., Brueton, L., Buckle, V.J., Burn, J., Clayton-Smith, J., Davison, B.C.C., Gardner, R.J.M., Homfray, T., Kearney, L., Kingston, H.M. *et al.* (1995) Clinical and hematologic aspects of the X-linked α-thalassemia/mental retardation syndrome (ATR-X). *Am. J. Hum. Genet.*, **55**, 288–299.
4. Wada, T., Sugie, H., Fukushima, Y. and Saitoh, S. (2005) Non-skewed X-inactivation may cause mental retardation in a female carrier of X-linked α-thalassemia/mental retardation syndrome (ATR-X): X-inactivation study of nine female carriers of ATR-X. *Am. J. Hum. Genet.*, **138A**, 18–20.
5. Gibbons, R.J., McDowell, T.J., Raman, S., O'Rourke, D.M., Garrick, D., Ayyub, H. and Higgs, D.R. (2000) Mutations in ATRX, encoding a SWI/SNF-like protein, cause diverse changes in the pattern of DNA methylation. *Nat. Genet.*, **24**, 361–371.
6. Wong, L.H., McGhie, J.D., Sim, M., Anderson, M.A., Ahn, S., Hannan, R.D., George, A.J., Morgan, K.A., Mann, J.R. and Choo, K.H.A. (2010) ATRX Interacts with H3.3 in maintaining telomere structural integrity in pluripotent embryonic stem cells. *Genome Res.*, **20**, 351–360.
7. Otani, J., Nankumo, T., Arita, K., Inamoto, S., Ariyoshi, M. and Shirakawa, M. (2009) Structural basis for recognition of H3K4 methylation status by the DNA methyltransferase 3A ATRX-DNMT3-DNMT3L domain. *EMBO Reports*, **10**, 1235–1241.
8. Dhayalan, A., Tamas, R., Bock, I., Tattermusch, A., Dimitrova, E., Kudithipudi, S., Ragozin, S. and Jeltsch, A. (2011) The ATRX-ADD domain binds to H3 tail peptides and reads the combined methylation state of K4 and K9. *Hum. Mol. Genet.*, **20**, 2195–2203.
9. Picketts, D.J., Higgs, D.R., Bachoo, S., Blake, D.J., Quarrell, O.W. and Gibbons, R.J. (1996) ATRX encodes a novel member of the SNF2 family of proteins: mutations point to a common mechanism underlying the ATR-X syndrome. *Hum. Mol. Genet.*, **5**, 1899–1907.
10. Eisen, J.A., Sweder, K.S. and Hanawalt, P.C. (1995) Evolution of the SNF2 family of proteins: subfamilies with distinct sequences and functions. *Nuc. Acids Res.*, **23**, 2715–2723.
11. Xue, Y., Gibbons, R., Yan, Z., Yang, D., McDowell, T.L., Sechi, S., Qin, J., Zhou, S., Higgs, D. and Wang, W. (2003) The ATRX syndrome protein forms a chromatin-remodeling complex with Daxx and localizes in promyelocytic leukemia nuclear bodies. *Proc. Natl Acad. Sci.*, **100**, 10635–10640.
12. Lewis, P.W., Elsaesser, S.J., Noh, K.-M., Stadler, S.C. and Allis, C.D. (2010) Daxx is an H3.3-specific histone chaperone and cooperates with ATRX in replication-independent chromatin assembly at telomeres. *Proc. Natl Acad. Sci.*, **107**, 14075–14080.
13. Drané, P., Ouararhni, K., Depaux, A., Shuaib, M. and Hamiche, A. (2010) The death-associated protein DAXX is a novel histone chaperone involved in the replication-independent deposition of H3.3. *Genes Dev.*, **24**, 1253–1265.
14. Ritchie, K., Seah, C., Moulin, J., Isaac, C., Dick, F. and Bérubé, N.G. (2008) Loss of ATRX leads to chromosome cohesion and congression defects. *J. Cell Biol.*, **180**, 315–324.
15. Garrick, D., Sharpe, J.A., Arkell, R., Dobbie, L., Smith, A.J., Wood, W.G., Higgs, D.R. and Gibbons, R.J. (2006) Loss of Atrx affects trophoblast development and the pattern of X-inactivation in extraembryonic tissues. *PLoS Genet.*, **2**, e58.
16. Bérubé, N.G., Mangelsdorf, M., Jagla, M., Vanderluit, J., Garrick, D., Gibbons, R.J., Higgs, D.R., Slack, R.S. and Picketts, D.J. (2005) The chromatin-remodeling protein ATRX is critical for neuronal survival during corticogenesis. *J. Clin. Invest.*, **115**, 258–267.
17. Bagheri-Fam, S., Argentaro, A., Svingen, T., Combes, A.N., Sinclair, A.H., Koopman, P. and Harley, V.R. (2011) Defective survival of proliferating Sertoli cells and androgen receptor function in a mouse model of the ATR-X syndrome. *Hum. Mol. Genet.*, **20**, 2213–2224.
18. Huh, M.S., Price O'Dea, T., Ouazia, D., McKay, B.C., Parise, G., Parks, R.J., Rudnicki, M.A. and Picketts, D.J. (2012) Compromised genomic integrity impedes muscle growth after Atrx inactivation. *J. Clin. Invest.*, **122**, 4412–4423.

19. Solomon, L.A., Li, J.R., Berube, N.G. and Beier, F. (2009) Loss of ATRX in chondrocytes has minimal effects on skeletal development. *PLoS ONE*, **4**, e7106.
20. Watson, L.A., Solomon, L.A., Li, J.R., Jiang, Y., Edwards, M., Shin-Ya, K., Beier, F. and Berube, N.G. (2013) Atrx deficiency induces telomere dysfunction, endocrine defects, and reduced life span. *J. Clin. Invest*, **123**, 2049–2063.
21. Seah, C., Levy, M.A., Jiang, Y., Mokhtarzada, S., Higgs, D.R., Gibbons, R.J. and Berube, N.G. (2008) Neuronal death resulting from targeted disruption of the Snf2 protein ATRX is mediated by p53. *J. Neurosci.*, **28**, 12570–12580.
22. Leung, J.W.-C., Ghosal, G., Wang, W., Shen, X., Wang, J., Li, L. and Chen, J. (2013) Alpha thalassemia/mental retardation syndrome X-linked gene product ATRX is required for proper replication restart and cellular resistance to replication stress. *J. Biol. Chem.*, **288**, 6342–6350.
23. Logan, M., Martin, J.F., Nagy, A., Lobe, C., Olson, E.N. and Tabin, C.J. (2002) Expression of Cre recombinase in the developing mouse limb bud driven by a Prxl enhancer. *Genesis*, **33**, 77–80.
24. Gibbons, R.J. (2006) Alpha thalassaemia-mental retardation, × linked. *Orphanet. J. Rare Dis.*, **1**, 1–15.
25. Gao, B., Hu, J., Stricker, S., Cheung, M., Ma, G., Law, K.F., Witte, F., Briscoe, J., Mundlos, S., He, L. *et al.* (2009) A mutation in Ihh that causes digit abnormalities alters its signalling capacity and range. *Nature*, **458**, 1196–1200.
26. Minami, Y., Oishi, I., Endo, M. and Nishita, M. (2010) Ror-family receptor tyrosine kinases in noncanonical Wnt signaling: their implications in developmental morphogenesis and human diseases. *Dev. Dyn.*, **239**, 1–15.
27. Oza, P., Jaspersen, S.L., Miele, A., Dekker, J. and Peterson, C.L. (2009) Mechanisms that regulate localization of a DNA double-strand break to the nuclear periphery. *Genes Dev.*, **23**, 912–927.
28. Soutoglou, E., Dorn, J.F., Sengupta, K., Jasin, M., Nussenzweig, A., Ried, T., Danuser, G. and Misteli, T. (2007) Positional stability of single double-strand breaks in mammalian cells. *Nat. Cell Biol.*, **9**, 675–682.
29. Aten, J.A., Stap, J., Krawczyk, P.M., van Oven, C.H., Hoebe, R.A., Essers, J. and Kanaar, R. (2004) Dynamics of DNA double-strand breaks revealed by clustering of damaged chromosome domains. *Science*, **303**, 92–95.
30. Schober, H., Ferreira, H., Kalck, V., Gehlen, L.R. and Gasser, S.M. (2009) Yeast telomerase and the SUN domain protein Mps3 anchor telomeres and repress subtelomeric recombination. *Genes Dev.*, **23**, 928–938.
31. Ahmed, E.A., Agay, D., Schrock, G., Drouet, M., Meineke, V. and Scherthan, H. (2012) Persistent DNA damage after high dose *in vivo* gamma exposure of minipig skin. *PLoS ONE*, **7**, e39521.
32. Lei, K., Zhu, X., Xu, R., Shao, C., Xu, T., Zhuang, Y. and Han, M. (2012) Inner nuclear envelope proteins SUN1 and SUN2 play a prominent role in the DNA damage response. *Curr. Biol.*, **22**, 1609–1615.
33. Johnson, B.R., Nitta, R.T., Frock, R.L., Mounkes, L., Barbie, D.A., Stewart, C.L., Harlow, E. and Kennedy, B.K. (2004) A-type lamins regulate retinoblastoma protein function by promoting subnuclear localization and preventing proteasomal degradation. Proc. Natl Acad. Sci. *USA*, **101**, 9677–9682.
34. Conte, D., Huh, M., Goodall, E., Delorme, M., Parks, R.J. and Picketts, D.J. (2012) Loss of Atrx sensitizes cells to DNA damaging agents through p53-mediated death pathways. *PLoS ONE*, **7**, e52167.
35. Maass, P.G., Rump, A., Schulz, H., Stricker, S., Schulze, L., Platzer, K., Aydin, A., Tinschert, S., Goldring, M.B., Luft, F.C. *et al.* (2012) A misplaced lncRNA causes brachydactyly in humans. *J. Clin. Invest.*, **122**, 3990–4002.
36. Williams, S.R., Aldred, M.A., Der Kaloustian, V.M., Halal, F., Gowans, G., McLeod, D.R., Zondag, S., Toriello, H.V., Magenis, R.E. and Elsea, S.H. (2010) Haploinsufficiency of HDAC4 causes brachydactyly mental retardation syndrome, with brachydactyly type E, developmental delays, and behavioral problems. *Am. J. Hum. Genet.*, **87**, 219–228.
37. Feldhahn, N., Ferretti, E., Robbiani, D.F., Callen, E., Deroubaix, S., Selleri, L., Nussenzweig, A. and Nussenzweig, M.C. (2012) The hSSB1 orthologue Obfc2b is essential for skeletogenesis but dispensable for the DNA damage response *in vivo*. *EMBO J.*, **31**, 4045–4056.
38. Wang, G., Woods, A., Agoston, H., Ulici, V., Glogauer, M. and Beier, F. (2007) Genetic ablation of Rac1 in cartilage results in chondrodysplasia. *Dev. Biol.*, **306**, 612–623.
39. Ulici, V., Hoenselaar, K.D., Agoston, H., McErlain, D.D., Umoh, J., Chakrabarti, S., Holdsworth, D.W. and Beier, F. (2009) The role of Akt1 in terminal stages of endochondral bone formation: angiogenesis and ossification. *Bone*, **45**, 1133–1145.
40. Vidaković, M., Koester, M., Goetze, S., Winkelmann, S., Klar, M., Poznanović, G. and Bode, J. (2005) Co-localization of PARP-1 and lamin B in the nuclear architecture: a halo-fluorescence- and confocal-microscopy study. *J. Cell. Biochem.*, **96**, 555–568.
41. Kuo, L.J. and Yang, L.-X. (2008) γ-H2AX - A novel biomarker for DNA double-strand breaks. *In Vivo*, **22**, 305–309.
42. Halawani, D., Mondeh, R., Stanton, L.A. and Beier, F. (2004) P38 MAP kinase signaling is necessary for rat chondrosarcoma cell proliferation. *Oncogene*, **23**, 3726–3731.
43. Meyer, O.A., Tilson, H.A., Byrd, W.C. and Riley, M.T. (1979) A method for the routine assessment of fore- and hindlimb grip strength of rats and mice. *Neurobehav. Toxicol. Teratol.*, **1**, 233–236.